Article

Changes in Dynamics of SRE-RNA on Binding to the VTS1p-SAM Domain Studied by C NMR Relaxation

Florian C. Oberstrass, Fre#de#ric H.-T. Allain, and Sapna Ravindranathan

J. Am. Chem. Soc., **2008**, 130 (36), 12007-12020 • DOI: 10.1021/ja8023115 • Publication Date (Web): 13 August 2008

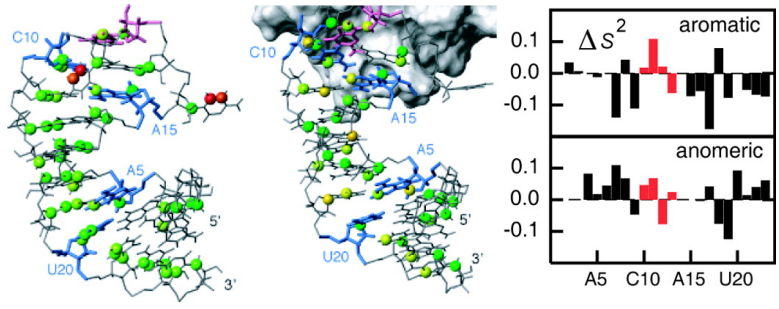

More About This Article

Additional resources and features associated with this article are available within the HTML version:

- Supporting Information
- Links to the 1 articles that cite this article, as of the time of this article download
- Access to high resolution figures
- Links to articles and content related to this article
- Copyright permission to reproduce figures and/or text from this article

View the Full Text HTML

Journal of the American Chemical Society is published by the American Chemical Society. 1155 Sixteenth Street N.W., Washington, DC 20036

J|A|C|S
ARTICLES

Published on Web 08/13/2008

Changes in Dynamics of SRE-RNA on Binding to the VTS1p-SAM Domain Studied by ^{13}C NMR Relaxation

Florian C. Oberstrass,[†] Frédéric H.-T. Allain,[†] and Sapna Ravindranathan*[,‡]

Institute of Molecular Biology and Biophysics, ETH Zurich, CH-8093 Zürich, Switzerland, and Central NMR Facility, National Chemical Laboratory, Pune 411008, India

Received March 30, 2008; E-mail: s.ravindranathan@ncl.res.in

Abstract: RNA recognition by proteins is often accompanied by significant changes in RNA dynamics in addition to conformational changes. However, there are very few studies which characterize the changes in molecular motions in RNA on protein binding. We present a quantitative ^{13}C NMR relaxation study of the changes in RNA dynamics in the pico−nanosecond time scale and micro−millisecond time scale resulting from interaction of the stem−loop SRE-RNA with the VTS1p-SAM domain. ^{13}C relaxation rates of the protonated carbons of the nucleotide base and anomeric carbons have been analyzed by employing the model-free formalism, for a fully $^{13}C/^{15}N$-labeled sample of the SRE-RNA in the free and protein-bound forms. In the free RNA, the nature of molecular motions are found to be distinctly different in the stem and the loop region. On binding to the protein, the nature of motions becomes more homogeneous throughout the RNA, with many residues showing increased flexibility at the aromatic carbon sites, while the anomeric carbon sites become more rigid. Surprisingly, we also observe indications of a slow collective motion of the RNA in the binding pocket of the protein. The observation of increased motions on binding is interesting in the context of growing evidence that binding does not always lead to motional restrictions and the resulting entropy gain could favor the free energy of association.

Introduction

Structural studies of RNA−protein interactions have shown that mutual accommodation by conformational adaptability of one or both components is an important aspect which governs how the intermolecular recognition takes place.[1−4] Since conformational adaptability implies structural movements in different parts of the protein and RNA, a detailed insight into the molecular basis for RNA−protein recognition is only possible by complementing the three-dimensional structural studies of RNA−protein complexes by detailed studies of molecular dynamics.

We report here a detailed ^{13}C NMR relaxation study of the role of RNA dynamics in the interaction of the Smaug recognition element stem−loop RNA (SRE-RNA) and the sterile alpha motif domain of *Saccharomyces cerevisiae* Vts1p (VTS1p-SAM). The SRE-RNA is a stem−loop RNA consisting of 23 nucleotides with a CUGGC pentaloop. The VTS1p-SAM domain adopts a globular fold comprised of six helices that are packed by a hydrophobic core. Recent solution state NMR and X-ray structural studies of the VTS1p-SAM domain, SRE-RNA and the protein−RNA complex indicate that the SAM domain recognizes the shape of the loop in the SRE-RNA.[5−7] In addition the nucleotide G which caps the pentaloop is base specifically recognized by a hydrophobic cavity formed by the protein.

Most NMR relaxation studies of dynamics involving RNA−protein recognition have focused on the changes which occur in protein dynamics on binding.[8−11] The reason for the larger body of work examining protein dynamics is that the methodology for analysis of NMR relaxation of ^{15}N nuclei in proteins is well established.[12] In RNA, on the other hand, the ^{13}C nuclei are better reporters of dynamics of the nucleotide base and sugar moieties of the individual residues. Quantitative analysis of ^{13}C relaxation data requires knowledge of ^{13}C chemical shift anisotropy (CSA) tensors. The orientation and magnitude of ^{13}C CSA tensors of the various carbons in RNA and DNA determined by solution state NMR methods have only become available recently.[13,14] The analysis of the relaxation of ^{13}C nuclei in RNA also becomes complicated in fully isotope-labeled systems by the presence of nearest neighbor $^{13}C-^{13}C$ dipolar interactions and detailed quantitative analysis of mo-

[†] ETH Zurich.
[‡] National Chemical Laboratory.

(1) Draper, D. E. *J. Mol. Biol.* **1999**, *293*, 255–270.
(2) Chen, Y.; Varani, G. *FEBS J.* **2005**, *272*, 2087–2097.
(3) Williamson, J. R. *Nat. Struct. Biol.* **2000**, *7*, 834–837.
(4) Leulliot, N.; Varani, G. *Biochemistry* **2001**, *40*, 7947–7956.
(5) Oberstrass, F. C.; Lee, A.; Stefl, R.; Janis, M.; Chanfreau, G.; Allain, F. H-T. *Nat. Struct. Biol.* **2006**, *13*, 160–167.
(6) Johnson, P. E.; Donaldson, L. W. *Nat. Struct. Biol.* **2006**, *13*, 177–178.
(7) Aviv, T.; Lin, Z.; Ben-Ari, G.; Smibert, C. A.; Sicheri, F. *Nat. Struct. Biol.* **2006**, *13*, 168–176.
(8) Jonker, H. R. A.; Ilin, S.; Grimm, S. K.; Wöhnert, J.; Schwalbe, H. *Nucleic Acids. Res.* **2007**, *35*, 441–454.
(9) Mittermaier, A.; Varani, L.; Muhandiram, D. R.; Kay, L. E.; Varani, G. *J. Mol. Biol.* **1999**, *294*, 967–979.
(10) Deka, P.; Paranji, P. K.; Perez-Canadillas, J. M.; Varani, G. *J. Mol. Biol.* **2005**, *347*, 719–733.
(11) Slijper, M.; Boelens, R.; Davis, A. L.; Konings, R. N. H.; Van Der Marel, G. A.; Van Boom, J. H.; Kaptein, R. *Biochemistry* **1997**, *36*, 249–254.
(12) Palmer, A. G., III *Chem. Rev.* **2004**, *104*, 3623–3640.
(13) Ying, J.; Grishaev, A.; Bryce, D. L.; Bax, A. *J. Am. Chem. Soc.* **2006**, *128*, 11443–11454.
(14) Bryce, D. L.; Grishaev, A.; Bax, A. *J. Am. Chem. Soc.* **2005**, *127*, 7387–7396.

10.1021/ja8023115 CCC: $40.75

lecular motions in such systems are fairly recent.[15−18] Detailed investigations of changes in RNA dynamics on binding to small ligands have been reported.[18,19] To our knowledge, however, only one recent study has examined the changes in RNA dynamics accompanying a protein recognition event.[20] Even though the dynamics of the free RNA has been analyzed quantitatively on the basis of motional models, the data analysis of the protein-bound RNA is based primarily on comparisons with observations in the free RNA. This study however provides valuable insights into the role of dynamics in the RNA−protein recognition event and is the only example where structural and dynamical aspects of the interaction have been examined for both binding partners.

In the present work, we extend the previous structural studies by characterizing the dynamics of SRE-RNA in its free form and when bound to the VTS1p-SAM domain (VTS1p−SRE-RNA). We report quantitative analysis of fast dynamical processes in the picosecond (ps) to nanosecond (ns) time scale and slow motions in the microsecond (μs) to millisecond (ms) time scale for SRE-RNA and VTS1p−SRE-RNA. Relaxation rate measurements at C2, C5, C6 and C8 sites of the nucleotide base and C1′ site of the ribose moieties have been carried out to obtain residue-specific dynamics information. Quantitative analysis of the relaxation data has been carried out employing the model-free formalism by including $^{13}C-^{13}C$ dipolar interactions and fully asymmetric CSA tensors recently reported for ^{13}C sites in nucleic acids.[13,14] Our results show that in the absence of the protein there is a clear distinction between the nature of motions in the loop and stem of SRE-RNA. On binding, this distinction is lost, but most residues, including a few which make important protein contacts, still retain their flexibility in the bound state. We also see evidence for a very dynamic interaction interface between the protein and RNA which probably involves collective slow motions.

Theory

^{13}C Relaxation. Relaxation of a ^{13}C spin is dominated by dipolar interaction with the directly attached proton and the ^{13}C CSA interaction with the static magnetic field. In RNA, there are several ^{13}C nuclei located in the nucleotide base and sugar moieties which can be studied by NMR relaxation techniques to probe molecular motion. Of these only C2 and C8 carbons of the G and A nucleotides with their directly bonded protons can be approximated as isolated two-spin systems in fully isotope labeled RNA samples. For such isolated spin systems the expressions for longitudinal and transverse relaxation rates and the heteronuclear NOE can be written in terms of spectral density functions involving C−H dipolar interaction and ^{13}C CSA.[21] The carbons C5, C6 and sugar carbons have neighboring ^{13}C nuclei; hence, additional terms involving $^{13}C-^{13}C$ dipolar interactions enter the relaxation rate expressions. In a uniformly labeled sample, C2 and C8 form $^{13}C_{2,8}-^{1}H_{2,8}$ spin systems, C6 and C1′ form $^{1}H_{6,1'}-^{13}C_{6,1'}-^{13}C_{5,2'}-^{1}H_{5,2'}$ spin systems and C5 forms $^{1}H_5-^{13}C_5-(^{13}C_4)-^{13}C_6-^{1}H_6$ spin system. The longitudinal relaxation rate is given by,[15,18,22]

$$R_1^C = \frac{1}{10}d_{CH}^2[(3J(\omega_C) + J(\omega_H - \omega_C) + 6J(\omega_H + \omega_C))] + \frac{1}{10}d_{CX}^2[J(\omega_X - \omega_C) + 3J(\omega_C) + 6J(\omega_X + \omega_C)] + \frac{2}{15}\Delta\sigma_{eff}^2\omega_C^2[3J(\omega_C)] \quad (1)$$

The transverse relaxation rate is,[15,18]

$$R_2^C = \frac{1}{20}d_{CH}^2[4J(0) + 3J(\omega_C) + J(\omega_H - \omega_C) + 6J(\omega_H) + 6J(\omega_H + \omega_C)] + \frac{1}{20}d_{CX}^2[5J(\omega_X - \omega_C) + 9J(\omega_C) + 6J(\omega_X + \omega_C)] + \frac{1}{45}\Delta\sigma_{eff}^2\omega_C^2[4J(0) + 3J(\omega_C)] + R_{ex} \quad (2)$$

The dipolar interaction constant is given by $d_{Ci} = (\mu_0/8\pi^2)(\gamma_C\gamma_i\hbar/r^3_{Ci})$, where $i = H,X$ and X represents nearest neighbor ^{13}C nuclei. The CSA tensor is not axially symmetric for the carbon nuclei in RNA and the effective anisotropy $\Delta\sigma_{eff}$, contributing to the relaxation is defined as,

$$\Delta\sigma_{eff} = \sqrt{(\sigma_{11} - \sigma_{33})^2 + (\sigma_{22} - \sigma_{33})^2 + 2(\sigma_{11} - \sigma_{33})(\sigma_{22} - \sigma_{33})} \quad (3)$$

where σ_{11}, σ_{22} and σ_{33} are the principal components of the CSA tensor, with σ_{11} denoting the least shielded component. The exchange rate R_{ex} in eq 2 accounts for the contribution to transverse relaxation from slow motions in the μs−ms time scale and has a quadratic dependence on the static field strength.

These expressions do not include cross correlation spectral density terms between dipolar and CSA interactions since the experimental schemes employed to measure the relaxation rates adequately suppresses the contributions from $^{13}C-^{1}H$ dipolar/^{13}C CSA cross-correlation effects by appropriate use of proton 180° pulses in the relaxation period.[22,23] Cross correlation terms involving $^{13}C-^{13}C$ dipolar interactions are 2−3 orders of magnitude smaller than the auto relaxation rates and maybe safely ignored.

For a typical spin system encountered in a fully labeled RNA sample, the expression for heteronuclear NOE also becomes more complicated. The C5, C6 and C1′ carbons are located in spin systems of the form $^{1}H-^{13}C-X-H'$ where X is a neighboring ^{13}C with a directly attached proton H′, and the expression for NOE is given by,[22]

$$\mathrm{NOE} = 1 + \left\{ \frac{\frac{R^{HC}}{R_1^C}\left(\frac{\gamma_H}{\gamma_C}\right) - \frac{R^{CX}R^{XH'}}{R_1^C R_1^X}\left(\frac{\gamma_{H'}}{\gamma_X}\right)}{1 - \frac{R^{CX^2}}{R_1^C R_1^X}} \right\} \quad (4)$$

The terms R^{HC} and R^{CX} are cross relaxation rates given by,

$$R^{Ci} = \frac{1}{10}d_{Ci}^2[6J(\omega_i + \omega_C) - J(\omega_i - \omega_C)] \quad (5)$$

(15) Boisbouvier, J.; Wu, Z.; Ono, A.; Kainosho, M.; Bax, A. *J. Biomol. NMR* **2003**, *27*, 133–142.
(16) Duchardt, E.; Schwalbe, H. *J. Biomol. NMR* **2005**, *32*, 295–308.
(17) Shajani, Z.; Varani, G. *J. Mol. Biol.* **2005**, *349*, 699–715.
(18) Hansen, A. L.; Al-Hashimi, H. M. *J. Am. Chem. Soc.* **2007**, *129*, 16072–16082.
(19) Dayie, K. T.; Brodsky, A. S.; Williamson, J. R. *J. Mol. Biol.* **2002**, *317*, 263–278.
(20) Shajani, Z.; Drobny, G.; Varani, G. *Biochemistry* **2007**, *46*, 5875–5883.
(21) Boisbouvier, J.; Brutscher, B.; Simorre, J.-P.; Marion, D. *J. Biomol. NMR* **1999**, *14*, 241–252.
(22) Yamazaki, T.; Muhandiram, R.; Kay, L. E. *J. Am. Chem. Soc.* **1994**, *116*, 8266–8278.
(23) Kay, L. E.; Nicholson, L. K.; Delaglio, F.; Bax, A.; Torchia, D. A. *J. Magn. Reson.* **1992**, *97*, 359–375.

where i = H,X. If ${R_1}^C = {R_1}^X$ and $R^{HC} = R^{XH'}$, the above expression for NOE simplifies to,

$$\mathrm{NOE} = 1 + \left(\frac{\gamma_H}{\gamma_C}\right)\left[\frac{R^{HC}}{R_1 + R^{CX}}\right] \tag{6}$$

Note that when R^{CX} is very small, as is the case when overall tumbling correlation time is <5 ns or in the absence of a neighboring carbon, the NOE expression becomes identical to the expression for an isolated ^{1}H$-^{13}$C two-spin system.

We now consider the relative significance of the ^{13}C$-^{13}$C dipolar interaction in the relaxation rates of the various carbon nuclei in the free RNA and protein-bound RNA. The major factors which determine the extent to which ^{13}C$-^{13}$C dipolar interaction contributes to relaxation are the correlation time for overall motion and the C$-$C internuclear distance along with the product of gyromagnetic ratios. Compared to r_{CH} interatomic distances of 1.08 Å (aromatic carbons) and 1.09 Å (anomeric carbon), the average r_{CC} distances are 1.36, 1.43 and 1.53 Å for C5$-$C6, C5$-$C4 and C1′$-$C2′ respectively.[15,16] For the 23-nucleotide SRE-RNA, the correlation time for overall motion is about 5 ns, and the ^{13}C$-^{13}$C dipolar interaction contribution to the relaxation rates is negligible compared to ^{13}C$-^{1}$H dipolar interaction and ^{13}C CSA.[15,17] For the VTS1p$-$SRE-RNA on the other hand, the RNA is bound to the protein and has a correlation time for overall motion that is nearly twice that of the free RNA. In this case, calculations show that there is a significant contribution from ^{13}C$-^{13}$C dipolar interactions to the R_1 rate which cannot be neglected. This is largely because of the spectral density term $J(\omega_X - \omega_C)$ in eq 1. This is essentially a zero frequency term which increases with correlation time and hence becomes significant for ^{13}C nuclei in large RNAs or RNA which is part of a macromolecular complex. The effect on R_2 rate is not as much because of the presence of a much larger zero frequency spectral density term involving the ^{13}C$-^{1}$H dipolar interaction which is more dominant. In calculations, we included ^{13}C$-^{13}$C dipolar interactions for all the rates of VTS1p$-$SRE-RNA but not for SRE-RNA.

The ^{13}C$-^{13}$C dipolar interaction also leads to the more complicated expression for NOE given above. This is because during proton irradiation in an NOE experiment, enhancement of intensity also occurs on the neighboring carbon which then transfers to the target carbon through the C$-$C cross relaxation process, which becomes more efficient at higher correlation times. Hence, the actual intensity increase observed at the target carbon during proton irradiation will be more than what is expected from transfer via its directly bonded proton alone and has to be calculated by including all relaxation rates of the extended spin system involving the neighboring carbon and its attached proton. For calculations of NOE in SRE-RNA the expression for an isolated two-spin system was employed. In the case of VTS1p$-$SRE-RNA, we employed the simplified version of the NOE expression in presence of ^{13}C$-^{13}$C dipolar interactions given by eq 6. The assumption that $R^{HC} = R^{XH'}$ and ${R_1}^C = {R_1}^X$ was verified by calculations assuming only overall motion. The difference in cross rates ($R^{H1'C1'} - R^{H2'C2'}$ and $R^{H5C5} - R^{H6C6}$) are in the range 0.001$-$0.01 s^{-1}, while the difference in corresponding ${R_1}^C$ rates was at most 0.2 s^{-1}.

Motional Models. In the case of nucleic acid molecules with long base-paired stems, the overall motion is usually described by an axially symmetric rotational diffusion tensor and the spectral density functions $J_{uv}(\omega)$ for a pair of interactions u and v in the relaxation rate equations are given by,[24,25]

$$J(\omega) = \sum_{a=0,2} C_a \frac{D_a}{D_a^2 + \omega^2} \tag{7}$$

where $D_a = 6D_\perp + a^2(D_\parallel - D_\perp)$. $D_\parallel$ and $D_\perp$ are the rotational diffusion constants for rotation about the long axis of the molecule and an axis perpendicular to it, respectively, and relate to the correlation time for overall motion as $\tau_c = (4D_\perp + 2D_\parallel)^{-1}$. The coefficients in the spectral density function are, $C_0 = 0.25(3\cos^2\theta_u - 1)(3\cos^2\theta_v - 1)$, $C_1 = 3\cos\theta_u\cos\theta_v\sin\theta_u\sin\theta_v\cos(\phi_u - \phi_v)$, $C_2 = 0.75\sin^2\theta_u\sin^2\theta_v\cos(2\phi_u - 2\phi_v)$.

In the relaxation rate equations, the dipolar interactions only have an auto correlated spectral density function for which $u = v$. The asymmetric CSA, however, is expressed in terms of two axially symmetric CSA tensors, and hence the spectral density function involving CSA interaction will also have a cross term with u and v corresponding to $(\sigma_{11} - \sigma_{33})$ and $(\sigma_{22} - \sigma_{33})$ respectively. The polar angles (θ_u,ϕ_u) and (θ_v,ϕ_v) define the orientations of the spin interactions with respect to the rotational diffusion tensor.

In the analysis of relaxation data of nuclei in biomolecules, the contribution from internal motions is introduced according to the model-free formalism which assumes that overall and internal motions occur independently of each other at widely differing time scales.[26] This separation is straightforward when the overall motion is described by isotropic rotational diffusion, and the total spectral density function is a sum of two terms weighted by an order parameter S^2 which is a measure of motional flexibility. Even though the separation is not straightforward when the overall motion is anisotropic, it is convenient to express global and internal motions within the framework of the well-established model-free formalism by defining the order parameter associated with each term in eq 7 in terms of a single order parameter S^2 for a specific interaction as, ${S_a}^2 = C_a S^2$. The total spectral density function then becomes,[27,28]

$$J_{uv}(\omega) = S^2 \sum_{a=0,2} C_a \frac{D_a}{D_a^2 + \omega^2} + (1 - S^2) \sum_{a=0,2} C_a \frac{D_{ai}}{D_{ai}^2 + \omega^2} \tag{8}$$

where S^2 is the order parameter for the corresponding spin interaction, and the terms incorporating internal motion correlation times is given by $D_{ai} = 6D_\perp + a^2(D_\parallel - D_\perp) + \tau_i^{-1}$ where τ_i is the correlation time for internal motion. An additional complication which arises in ^{13}C interactions in RNA is that the ^{1}H$-^{13}$C dipolar interaction, ^{13}C$-^{13}$C dipolar interaction and components of the asymmetric CSA do not coincide. This implies that ideally a separate set of S^2, τ_i parameters should be defined for each interaction. The approximation used in eq 8 which employs the same S^2 and τ_i values for all interactions of a given ^{13}C spin can be justified when considering the relative

(24) Woessner, D. E. *J. Chem. Phys.* **1962**, *3*, 647–654.
(25) Schwalbe, H.; Carlomagno, T.; Hennig, M.; Junker, J.; Reif, B.; Richter, C.; Griesinger, C. *Methods Enzymol.* **2001**, *338*, 35–81.
(26) Lipari, G.; Szabo, A. *J. Am. Chem. Soc.* **1982**, *104*, 4546–4558.
(27) Barbato, G.; Ikura, M.; Kay, L. E.; Pastor, R. W.; Bax, A. *Biochemistry* **1992**, *31*, 5269–5278.
(28) Akke, M.; Fiala, J. F.; Patel, D.; Palmer, A. G., III *RNA* **1997**, *3*, 702–709.

contributions of the various interactions to the relaxation rates (discussed further below).

Materials and Methods

Protein, RNA and Complex Preparation. The SAM domain of *S. cerevisiae* Vts1p has been expressed and purified as previously described.[5] *Escherichia coli* host cells BL21(DE3)+RIL (Stratagene) were grown in M9 medium containing $^{15}NH_4Cl$ as nitrogen source for ^{15}N labeling of the protein samples. After purification the proteins were dialyzed against NMR-Buffer (50 mM NaCl, 20 mM NaH_2PO_4, pH 6.5) and concentrated. For this study, a 23 nucleotide long RNA stem−loop (5′-GGAGAGGCUCUGGCAGC-UUUUCC-3′) with two different labeling schemes was used (either G and C or A and U being ^{13}C ^{15}N-labeled). RNA samples were produced by *in vitro* T7 polymerase runoff transcription and purified by anion-exchange HPLC under denaturing conditions. The RNA oligonucleotides were annealed in NMR-Buffer (50 mM NaCl, 20 mM NaH_2PO_4, pH 6.5) by heating to 95 °C and snap cooling on ice to favor a stem−loop conformation. For complex formation proteins and RNAs were mixed with a 1:1 ratio. Concentrations were determined by UV spectroscopy ($\epsilon_{prot,280} = 16500\ M^{-1}\ cm^{-1}$; $\epsilon_{RNA,260} = 217300\ M^{-1}\ cm^{-1}$). All samples used for NMR spectroscopy were approximately 1 mM.

NMR Spectroscopy. Longitudinal relaxation rates (R_1), transverse relaxation rates in the rotating frame ($R_{1\rho}$) and heteronuclear NOE measurements were carried out for C2, C5, C6, C8 and C1′ carbons in two sets of SRE-RNA and VTS1p−SRE-RNA samples, with isotope labeling of G,U residues in the first set and A,C residues in the second.

Standard pulse sequences involving an INEPT transfer, a variable relaxation period, ^{13}C frequency labeling and final INEPT transfer for proton detection, were employed for relaxation rate measurements of the C2 and C8 carbons which do not have ^{13}C neighbors.[23,29] R_1 relaxation was sampled at time points 20, 40, 80, 160, 240, 340, 480, 800, 1000 ms and $R_{1\rho}$ relaxation was sampled at 4, 8, 12, 16, 24, 32, 40 ms with repeat measurements at two time points in both cases. In the case of VTS1p−SRE-RNA sample the $R_{1\rho}$ relaxation was sampled for shorter delays (4, 8, 12, 16, 20, 24, 28 ms) because of faster relaxation in the RNA−protein complex. The NOEs were measured from spectra recorded with and without proton presaturation using a total relaxation delay of 5 s, in which proton irradiation was applied for 3 s in the former.

For measurements on C5, C6 and C1′ carbons with ^{13}C neighbors, the standard pulse sequences were modified to include a selective ^{13}C 180° IBURP-shaped pulse during the first INEPT transfer to allow selective excitation of the desired carbon resonance. In addition the ^{13}C frequency labeling was implemented with a constant-time evolution period set to n/J_{CC} ms where J_{CC} is the scalar coupling between directly bonded carbons.[15,17,22] In experiments on the SRE-RNA sample $n = 2$ was used for C5 and C6 carbons and n was set to 1 for C1′ carbon. In the VTS1p−SRE-RNA sample, n was set to 1 for all carbons to minimize relaxation losses resulting from fast transverse relaxation in the complex. The time points for R_1 measurements were set to 20, 40, 80, 120, 240, 340, 480, 800, 1000 ms and the $R_{1\rho}$ measurements were carried out for time points 4, 8, 12, 16, 20, 24, 28 ms with additional time points at 40 and 48 ms included for the slower relaxing C1′ carbons. For the VTS1p−SRE-RNA sample, the last time points were omitted. Both SRE-RNA and VTS1p−SRE-RNA have modest molecular masses of about 8 and 16 kDa so that spectra with fairly good signal-to-noise ratios could be obtained on a low temperature probe; hence, TROSY enhanced sequences[18] were not employed in the measurements.

In the $R_{1\rho}$ experiments a spin-lock field strength of 3 KHz was employed with the carrier positioned at the center of the ^{13}C resonance region of interest and taking care to avoid Hartmann−Hahn type magnetization transfers. Since the different pairs of scalar coupled carbons resonate in distinct spectral regions, $R_{1\rho}$ can be measured for C6, C5 and C1′ without interference from unwanted magnetization transfers. Nonzero offsets of individual resonances causes the measured $R_{1\rho}$ values to have contributions from R_1 in addition to $R_{1\rho}$. The true $R_{1\rho}$ values were extracted according to $R_{1\rho}\ (measured) = R_1 \cos^2\beta + R_{1\rho} \sin^2\beta$, in which $\beta = \arctan(\nu_{SL}/\Omega)$ is the effective tilt angle of the spin-lock field, with ν_{SL} and Ω being the spin-lock field strength and resonance offset in Hz respectively.[30] $R_{1\rho}$ measurements were also carried out at 1, 2, 4.5 and 6 KHz to examine spin-lock dependence of relaxation rates resulting from slow motions.

The $^{13}C-^{1}H$ correlation experiments were carried out with 200 × 1024 points for relaxation rate measurements on C2 and C8 carbons. Experiments on C5 and C6 carbons of SRE-RNA were carried out with 224 × 1024 points, whereas 176 × 1024 points were used for C1′ carbon. In the VTS1p−SRE-RNA sample the data matrix was 80 × 1024 points for C5, C6 carbons and 170 × 1024 for C1′ carbon. Sufficient resolution of resonances were obtained in all cases since each sample used had isotope labels on only two nucleotide types, thereby reducing spectral overlap. The ^{1}H carrier was set on the residual water resonance, while the ^{13}C carrier frequency was set to the center of the carbon resonance region of interest (C2,C8: 135.3 ppm, C6: 139.8 ppm, C5: 101.5 and 93.5 ppm respectively for G,U and A,C labeled samples, C1′: 89.5 ppm).

Experiments were carried out on a DRX Bruker 500 MHz spectrometer equipped with a 5 mm triple resonance cryogenic probe and an Avance II Bruker 600 MHz spectrometer with 5 mm triple resonance TXI probe. All measurements were carried out at 303 K.

All numerical calculations were carried out using in-house Fortran software implementing the general computational strategy employed for model-free analysis in proteins.[31] The calculations are based on the equations in the text and include $^{13}C-^{1}H$ dipolar, nearest neighbor $^{13}C-^{13}C$ dipolar and fully asymmetric CSA interactions. The asymmetric CSA tensors were incorporated into the calculation of relaxation rates by decomposing into a sum of two axially symmetric CSA contributions.[32] The magnitudes and orientations reported recently for the CSA tensors of aromatic and anomeric carbons have been employed in numerical calculations.[13,14] The CSA tensors have been determined for an A-form RNA helix which favors a C3′ endo sugar conformation; hence. these values are approximate when applied to anomeric carbons of the C10 and U11 residues of SRE-RNA which have ribose moieties in C2′ endo conformation. Density functional theory calculations predict a slightly higher CSA for anomeric carbons in a C2′ endo sugar.[33] Since dipolar interactions largely dominate relaxation of C1′ carbons, the use of CSA tensors of C3′ endo sugars in the calculations is unlikely to affect the estimation of dynamics parameters of C1′ carbons in C10 and U11 residues significantly.

Standard C−H and C−C bond lengths (see Theory section) have been employed in all calculations. In more recent work, the use of motionally averaged C−H distances (1.102 or 1.104 Å for aromatic sites and 1.118 or 1.115 Å for anomeric sites) in the analysis of ^{13}C relaxation data in RNA has been suggested.[18,34] Incorporation of these longer bond distances results in an increase of estimated order parameters by 10% on average for aromatic sites and 16% for anomeric sites when compared to estimates employing standard bond lengths. For several residues, the use of motionally averaged C−H distances thus results in S^2 parameters exceeding unity which is contrary to its definition ($0 \le S^2 \le 1$). A similar observation on

(29) Peng, J. W.; Wagner, G. *J. Magn. Reson.* **1992**, *98*, 308–332.
(30) Akke, M.; Palmer III, A. G. *J. Am. Chem. Soc.* **1996**, *118*, 911–912.
(31) Mandel, A. M.; Akke, M.; Palmer, A. G., III *J. Mol. Biol.* **1995**, *246*, 144–163.
(32) Goldman, M. *J. Magn. Reson.* **1984**, *60*, 437–452.
(33) Dejaegere, A. P.; Case, D. P. *J. Phys. Chem. A* **1998**, *102*, 5280–5289.
(34) Ferner, J.; Villa, A.; Duchardt, E.; Widjajakusuma, E.; Wöhnert, J.; Stock, G.; Schwalbe, H. *Nucleic Acids. Res* **2008**, *36*, 1928–1940.

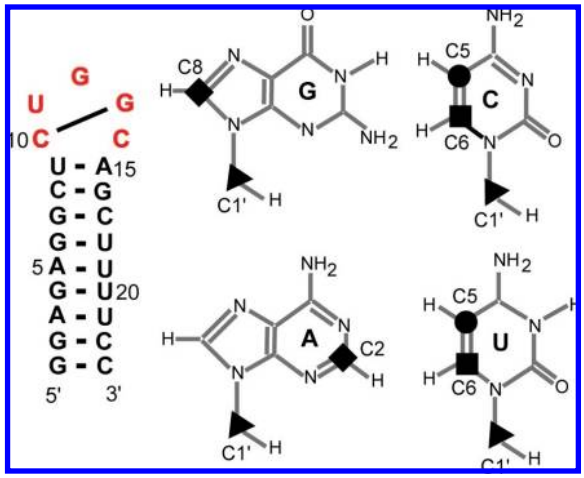

Figure 1. Secondary structure of the 23-nucleotide SRE-RNA with the protein recognition loop indicated in red. The carbon relaxation probes employed for dynamics studies are also indicated.

using larger r_{CH} distances has been reported and the discrepancy in the case of aromatic carbons has been explained on the basis of an underestimation of CSA magnitudes employed in the calculations.[16,34] However, in the case of C1′ carbons for which CSA contribution to relaxation is very small, the reason for S^2 values exceeding unity is not clear.[16] Here we retain standard C−H bond lengths in all calculations for estimating parameters relating to molecular dynamics. Comparing results from calculations employing both sets of bond distances show that the relative variations of estimated parameters among the different residues and changes observed between SRE-RNA and VTS1p−SRE-RNA are unaffected. Hence, the conclusions regarding the nature of motions at different sites in the RNA and changes resulting from binding to the protein are not influenced by the use of standard C−H distances. The molecular structure coordinates required for the calculations are available in the protein data bank with accession codes 2ES5 (SRE-RNA) and 2ESE (VTS1p−SRE-RNA).

Results and Discussion

Dynamics Studies of SRE-RNA. The 23-nucleotide RNA construct employed in this study is shown in Figure 1. By using two sets of identical samples, one with isotope labels only in G,U nucleotides and the other with labels only in A,C nucleotides, reliable ^{13}C relaxation rates could be extracted for all C2, C5, C6, C8 and C1′ carbons. The only exceptions are the C8 carbons of residues G4 and G6 which are overlapped and the carbons of residue G1. The measured relaxation rates R_1, $R_{1\rho}$ and ^{1}H−^{13}C NOE are shown in Figure 2 (rates for C6 carbons are in Figure S1). The data were analyzed to extract information about global motion, fast internal motion and slow conformational fluctuations.

Global Motion. In order to characterize overall motion described by an axially symmetric diffusion tensor, four parameters have to be determined, namely a correlation time which is related to rotational diffusion constants, $\tau_c = (4D_\perp + 2D_{||})^{-1}$, the ratio of the diffusion constants $D_{||}/D_\perp$ and the polar angles which define the orientation of the unique axis ($D_{||}$ axis) of the diffusion tensor with respect to the PDB frame of the molecular structure.

The strategy of extracting rotational diffusion tensor parameters from the ratio of relaxation rates $R_{1\rho}/R_1$ is well established and has been applied to proteins and nucleic acids.[15,35]In the absence of significant fast internal motions and slow conformational exchange, this ratio depends only

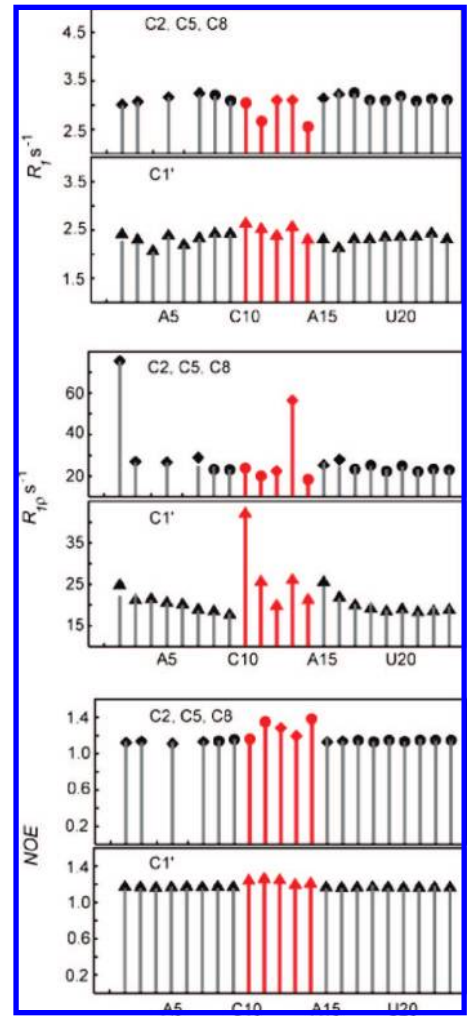

Figure 2. Experimental relaxation rates (symbols) and rates calculated (bars) using axially symmetric rotational diffusion model with internal motion parameters given in Table 1, for C2, C5, C8 and C1′ carbons of SRE-RNA at 500 MHz.

on parameters relating to overall motion. Fast internal motions and conformational exchange are typically observed in RNA for end residues and those in internal loops.[16,17] The experimental data in Figure 2 shows higher $R_{1\rho}$ rates and NOEs for residues in the loop region indicative of the presence of slow conformational exchange and fast internal motions. The $R_{1\rho}$ relaxation rates of some of the residues in the loop region also show a dependence on the spin-lock field strength, indicative of slow motions in the μs−ms time scale (discussed below). After excluding data from the end residues and loop residues, 39 $R_{1\rho}/R_1$ ratios from aromatic and anomeric carbons were employed in determining parameters for overall motion. Accurate characterization of the diffusion tensor requires data from ^{13}C sites which have a wide distribution of C−H bond orientations with respect to the $D_{||}$ axis. The base planes are mostly perpendicular to the $D_{||}$ axis and have a narrow distribution of C−H bond orientations whereas the anomeric carbons of the sugars expand the distribution over a much wider angular range.

(35) Tjandra, N.; Feller, S. E.; Pastor, R. W.; Bax, A. *J. Am. Chem. Soc.* **1995**, *117*, 12562–12566.
(36) Garcia de la Torre, J.; Huertas, M. L.; Carrasco, B. *J. Magn. Reson.* **2000**, *147*, 138–146.

Table 1. Internal Motion Parameters for SRE-RNA

	C2/C6/C8			C5			C1′		
	S^2	τ_i (ps)	R_{ex} (s^{-1})	S^2	τ_i (ps)	R_{ex} (s^{-1})	S^2	τ_i (ps)	R_{ex} (s^{-1})
G2	0.966 ± 0.015		50.5 ± 0.90				1.0		
A3	0.901 ± 0.007		1.0 ± 0.12				1.0		
G4	*overlap*						0.918 ± 0.011		0.6 ± 0.03
A5	0.890 ± 0.007		1.9 ± 0.11				0.982 ± 0.009	36.3 ± 4.0	
G6	*overlap*						0.883 ± 0.009		2.0 ± 0.11
G7	1.0						0.891 ± 0.011		1.4 ± 0.06
C8	0.953 ± 0.006			0.957 ± 0.008			0.933 ± 0.012		
U9	0.934 ± 0.007		2.4 ± 0.14	0.908 ± 0.007	16.2 ± 1.0		0.927 ± 0.012		
C10	0.971 ± 0.008	81.3 ± 5.0		0.878 ± 0.009	14.5 ± 1.5	1.3 ± 0.07	0.954 ± 0.009	147 ± 2.9	23.4 ± 0.23
U11	0.654 ± 0.008	44.1 ± 1.2	2.3 ± 0.12	0.696 ± 0.006	47.1 ± 1.4	1.5 ± 0.14	0.932 ± 0.011	106 ± 2.5	6.8 ± 0.13
G12	0.866 ± 0.010	82.9 ± 1.7					0.926 ± 0.013	56.8 ± 1.2	
G13	0.947 ± 0.009	87.2 ± 2.0	31.9 ± 0.13				0.945 ± 0.008	29.8 ± 0.9	7.9 ± 0.13
C14	0.650 ± 0.005	46.9 ± 1.3		0.682 ± 0.008	55.4 ± 1.2		0.960 ± 0.007	56.2 ± 1.1	
A15	0.905 ± 0.009	35.5 ± 1.9					1.0		1.9 ± 0.07
G16	1.0						0.930 ± 0.009		1.2 ± 0.09
C17	0.990 ± 0.007			0.963 ± 0.037	34.1 ± 1.6		0.958 ± 0.011		
U18	0.959 ± 0.006			0.921 ± 0.007		1.6 ± 0.14	0.958 ± 0.011	41.0 ± 2.0	
U19	0.957 ± 0.008			0.909 ± 0.004	17.3 ± 2.0		0.934 ± 0.008		
U20	0.946 ± 0.009			0.957 ± 0.009			0.908 ± 0.009		1.1 ± 0.13
U21	0.933 ± 0.005	25.9 ± 3.0		0.903 ± 0.007	19.9 ± 1.0		0.927 ± 0.006		
C22	0.939 ± 0.006	13.4 ± 2.0		0.925 ± 0.007			0.960 ± 0.006	31.9 ± 2.0	
C23	0.919 ± 0.007	46.6 ± 2.0		0.920 ± 0.006			0.939 ± 0.007		

The global motion parameters were obtained by minimizing the difference between experimental and calculated ratios,

$$\chi^2 = \sum_{i=1,N} \left[\frac{(R_{1\rho}/R_1)_i^{exp} - (R_{1\rho}/R_1)_i^{cal}}{\sigma_i} \right]^2 \quad (9)$$

where σ_i is the estimated error in the experimental ratio denoted by superscript *exp* and the ratio denoted by superscript *cal* are calculated using eqs 1, 2 and 7 setting exchange rate R_{ex} to zero. Fully asymmetric CSA tensors for the aromatic and anomeric carbons determined recently for nucleic acids were employed in these calculations.[13,14] The orientation ($\theta_{||}$, $\phi_{||}$) of the $D_{||}$ axis was scanned by a grid search of 1° steps and at each point the best fit parameters τ_c and $D_{||}/D_\perp$ were determined by employing Powell downhill minimization algorithm. The grid search gives a minimum at ($\theta_{||}$, $\phi_{||}$) = (77°, 112°) with a corresponding overall rotational correlation time τ_c = 4.27 ns and a diffusion anisotropy of $D_{||}/D_\perp$ = 1.49 (Figure S2). These values agree fairly well with the values of ($\theta_{||}$, $\phi_{||}$) = (85°, 109°), τ_c = 4.14 ns and $D_{||}/D_\perp$ = 1.34 obtained from hydrodynamic calculations using the program *hydronmr*.[36,37] The rotational diffusion anisotropy of 1.49 also agrees with the value of 1.55 determined from the ratio of the principal components of the inertia tensor.

Internal Motions. Knowledge of the parameters defining overall motion allows the relaxation data to be analyzed by the model-free formalism to extract information about residue specific local motions at the individual ^{13}C sites. The three experimental relaxation data measured for each ^{13}C site were analyzed in terms of four internal motion models of increasing complexity and number of parameters; (1) S^2 (2) S^2, τ_i (3) S^2, R_{ex} (4) S^2, τ_i, R_{ex}. Here, S^2 is a measure of the amplitude of the internal motions, with a lower extreme value of zero signifying high flexibility and a value of one at the other extreme implying rigidity. The correlation time for these fast internal motions, τ_i, is of the order of 10−200 ps. The parameter R_{ex} is an additional contribution to transverse relaxation in the presence of slow conformational fluctuations in the μs−ms time scale.

The parameters for internal motion corresponding to each of the four models were determined by minimizing the target function for each ^{13}C,

$$\chi^2_{int} = \left[\frac{R_1^{exp} - R_1^{cal}}{\sigma_{R_1}} \right]^2 + \left[\frac{R_{1\rho}^{exp} - R_{1\rho}^{cal}}{\sigma_{R_{1\rho}}} \right]^2 + \left[\frac{\mathrm{NOE}^{exp} - \mathrm{NOE}^{cal}}{\sigma_{\mathrm{NOE}}} \right]^2 \quad (10)$$

In the above expression, rates were calculated using eqs 1, 2, 6 and 8 with the global motion parameters fixed to the values determined from the ratios of relaxation rates. The choice of the most suitable model for each ^{13}C site was made by comparing the quality of fits to each of the four models by employing Akaike's information criterion[38] and the parameters that best describe the dynamics at each ^{13}C site are given in Table 1. The relaxation rates calculated using these parameters are included along with the plots of experimental data in Figure 2.

As mentioned in the theoretical section, a rigorous analysis of fast motions would require the use of different sets of internal motion parameters S^2 and τ_i corresponding to the motions of the C−H dipolar vector, C−C dipolar vector and the CSA components at each site, since their directions do not coincide. Our analysis however uses an approximation which describes local motion at each site in terms of the same S^2 and τ_i values for all interactions and has also been employed in other dynamics studies of RNA.[16,18] We carried out an estimation of the extent to which the use of a single S^2 and τ_i for all interactions at a given ^{13}C site can be justified. The C−H dipolar interaction and one of the CSA components (least shielded) are closely aligned as in the case of the corresponding interactions of ^{15}N nuclei in proteins. Together these two contribute about 86% to the relaxation of aromatic carbons and almost 97% to the relaxation of anomeric carbons. Hence the approximation of a single S^2 and τ_i value should adequately reflect the local motions at each ^{13}C site.

Most of the residues in the stem region have very fast internal motions with time scales less than 10 ps so that the relaxation

(37) Fernandes, M. X.; Ortega, A.; López Martinez, M. C.; Garcia de la Torre, J. *Nucleic Acids. Res.* **2002**, *30*, 1782–1788.

(38) d'Auvergne, E. J.; Gooley, P. R. *J. Biomol. NMR* **2003**, *25*, 25–39.

data can be accounted for in terms of the order parameter S^2. The ^{13}C sites of the loop and flanking residues on the other hand, have fast internal motions with correlation times ranging from about 30−100 ps and the fits to relaxation data are obtained with more complex models of internal motion (models 2 and 4). This suggests that the nature of fast internal motions is distinctly different in the stem and loop regions.

For the ^{13}C sites in the nucleotide base, the amplitude of fast motions as defined by the S^2 values, show variations between stem and loop region. With the exception of C10 and G13 residues, S^2 values are significantly lower in the loop region compared to the stem. It is interesting that the C10 and G13 residues are hydrogen bonded across the loop and have S^2 values similar to those for the base-paired residues in the stem. Residues U11 and C14 have much lower S^2 values indicating a high level of local flexibility whereas the G12 residue which stacks over the C10-G13 base pair, has an S^2 value which is intermediate between the more rigid C10-G13 pair and the highly flexible U11, C14 residues.

The observed relative flexibility of the different residues is consistent with the solution structure of the SRE-RNA.[5] Base-pairing between the C10 and G13 residues in the loop was suggested in the SRE-RNA structure and is supported by the similarity of the S^2 parameters of C10 and G13 to those of the base-paired residues in the stem. The higher S^2 values observed for the aromatic sites of C10, G12 and G13 along with the anomeric sites of the loop residues, supports the idea that the loop adopts a well-defined structure that aids shape specific recognition by the VTS1p-SAM domain. The nucleotide base planes of the U11 and C14 residues are seen to project outward from the sugar−phosphate backbone in the structure. The much lower S^2 values observed for the aromatic carbons of these residues indicate a high degree of motional freedom. The nucleotide base in U11 and C14 are like side groups attached to the sugar−phosphate backbone, and high amplitude motions about the glycosidic linkage is feasible. In contrast to the ^{13}C sites in the nucleotide base, the anomeric sites do not show significant differences in S^2 values between the loop and stem region.

Slow Conformational Fluctuations. The presence of slow motions in the μs−ms time scale leads to an increase in the transverse relaxation rate by a factor R_{ex}. Resonances that exhibit slow motions in this time scale will show a decrease in $R_{1\rho}$ relaxation rates as the power of the spin-lock field is increased. The dependence of the transverse relaxation rates of ^{13}C nuclei exchanging between two sites ($R_{1\rho}^{ex}$), on the spin-lock field strength is given by,[30,39]

$$R_{1\rho}^{ex} = R_1 \cos^2\beta + R_2 \sin^2\beta + p_1 p_2 \Delta\omega^2 \sin^2\beta \frac{\tau_{ex}}{1+\omega_e^2\tau_{ex}^2} \quad (11)$$

where β is the tilt angle of the spin-lock field as defined in the methods section and the effective field, $\omega_e = (\Delta\omega_o{}^2 + \omega_{SL}{}^2)^{0.5}$, is expressed in terms of the spin-lock carrier offset with respect to the exchange averaged resonance position ($\Delta\omega_o$) and the field strength, ω_{SL} in radians/s. The parameter τ_{ex} is the exchange time constant characterizing exchange between two sites with fractional populations p_1 and p_2. The chemical shift difference between the two sites is given by $\Delta\omega$.

(39) Davis, D. G.; Perlman, M. E.; London, R. E. *J. Magn. Reson. B* **1994**, *104*, 266–275.

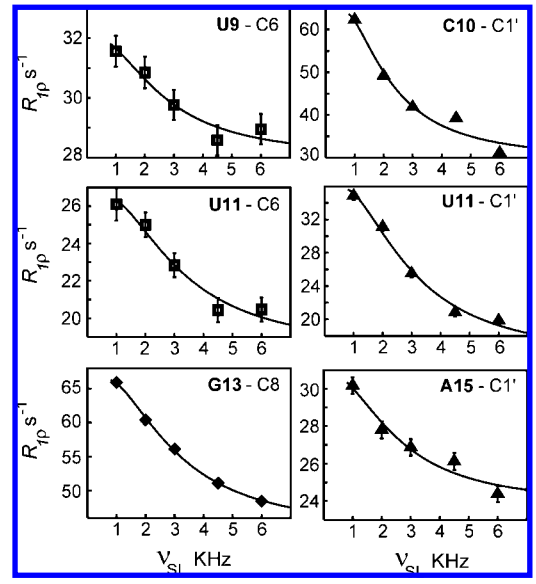

Figure 3. Fits of the two-site fast exchange model to the spin-lock field strength dependence of $R_{1\rho}$ rates for aromatic and anomeric carbons of SRE-RNA.

The spin-lock field strength dependence of $R_{1\rho}$ rates observed for some of the ^{13}C sites in SRE-RNA is shown in Figure 3. This observation confirms that the residues in which these ^{13}C nuclei are located are undergoing conformational fluctuations on slow time scales. The same ^{13}C nuclei were also found to have significant slow exchange contributions in the model free analysis as seen from the corresponding R_{ex} parameters in Table 1. Figure 3 also includes fits to the experimental data based on eq 11, in which the product ($p_1p_2\Delta\omega^2$), R_2 and τ_{ex} are treated as fit parameters (Table S1). Model-free analysis of relaxation rates and spin-lock field dependence studies indicates that the residues which experience slow motions in the μs-ms time scale are mostly located in the loop and flanking residues with the exception of G2. The largest slow exchange contributions are observed for the residues G2 and G13 which are located at the edges of the base-paired region possibly undergoing slow opening and closing of the base pairs. Of the residues in the loop, exchange contribution to relaxation is observed for C10, U11 and G13. The sugar moieties of C10 and U11 have a 2′ endo conformation, and in the case of G13, a weak H1′−H2′ cross peak is observed in the TOCSY spectrum suggesting a conformational equilibrium between C2′ and C3′ endo conformations.

Dynamics Studies of VTS1p−SRE-RNA. The SRE-RNA bound to the VTS1p-SAM domain has approximately twice the molecular weight as the unbound RNA. Even in the bound form the macromolecular complex has a modest molecular weight of about 16 kDa, and ^{13}C relaxation rates can be measured reliably for most of the residues. As in the case of SRE-RNA, two sets of samples with isotope labeling on only two nucleotide types per sample were used for the experiments. For the C6 carbons, relaxation rates (R_1 and $R_{1\rho}$) were measured only for the AC labeled sample since several of the C6 resonances were overlapped in the GU labeled sample. The C6 carbon data were therefore not included in the analysis of internal motions. The experimental rates measured for C2, C5, C8 and C1′ carbons at 500 MHz are shown in Figure 4. When compared to SRE-RNA, the R_1 relaxation rates decrease, whereas the $R_{1\rho}$ rates increase as expected for an increase of correlation time for overall motion.

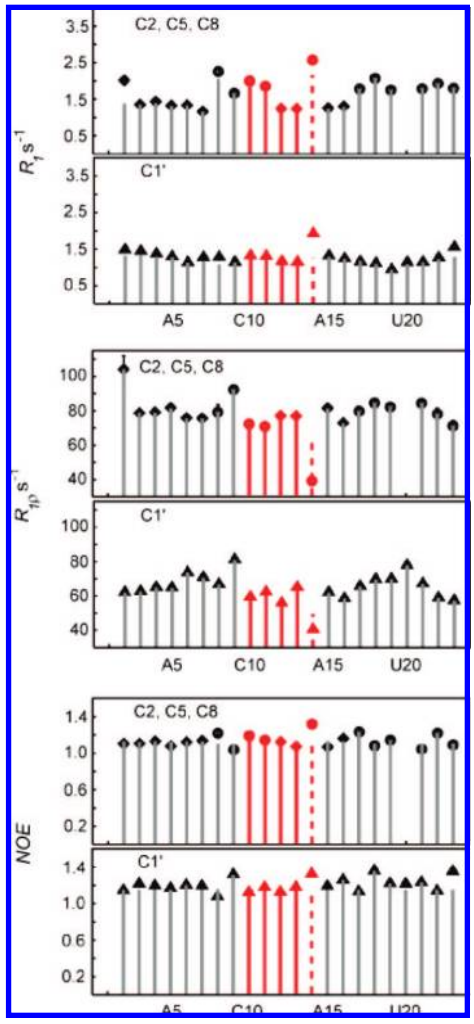

Figure 4. Experimental relaxation rates (symbols) and rates calculated (bars) using the axially symmetric rotational diffusion model with internal motion parameters given in Table 2, for C2, C5, C8 and C1′ carbons of VTS1p−SRE-RNA at 500 MHz. Internal motion parameters were not determined for residue C14 and the dashed line corresponds to the rates calculated assuming only global motion.

Global Motion. In order to extract parameters corresponding to overall motion from the $R_{1\rho}/R_1$ ratios, the data points from residues with fast internal motions and slow exchange have to be excluded. Experiments for examining spin-lock field dependence of $R_{1\rho}$ rates indicate the presence of slow motions for many of the residues of the RNA in the bound state (see below). In addition we compared the relaxation data obtained at 500 and 600 MHz for the anomeric carbons, shown in Figure S3. The R_1 rates decrease at the higher field strength and is consistent with the expected decrease of about 25% for a molecule with correlation time of about 10 ns when the static field changes from 500 to 600 MHz. The corresponding increase in $R_{1\rho}$, however, is more than can be accounted for merely by an increase of static field strength. The R_1 rates depend on high frequency spectral density terms which decrease at higher magnetic field and hence accounts for the drop in rates. $R_{1\rho}$ on the other hand is dominated by the zero frequency spectral density function which is field independent. Also the dominant relaxation mechanism for C1′ carbon relaxation is dipolar interaction with a negligible contribution from the field dependent CSA interaction. Hence the increase in $R_{1\rho}$ values with a change in static field from 500 to 600 MHz should be negligibly small (0.1 − 0.2%). The unexpectedly large difference which is observed for the $R_{1\rho}$ rates can be accounted for only by assuming the presence of a R_{ex} term which scales quadratically with the field strength.

For the aromatic carbons, increases in $R_{1\rho}$ rates with static field cannot be attributed to exchange alone because the CSA contributes substantially to relaxation and is field dependent. In order to obtain more insights into the extent of the exchange contribution, we calculated the relaxation rates for all ^{13}C sites in the absence of internal motions using global motion parameters obtained from hydrodynamic calculations. The difference between experimental and calculated relaxation rates (ΔR_1 and $\Delta R_{1\rho}$) is compared in Figure 5 for both SRE-RNA and VTS1p−SRE-RNA. For SRE-RNA both ΔR_1 and$\Delta R_{1\rho}$ lie close to zero for most residues, with slight deviations between residues arising from internal motions. Larger deviations from zero are observed only in the case of residues located mostly in the loop region which have contributions from slow exchange. In VTS1p−SRE-RNA, ΔR_1 values are close to zero but $\Delta R_{1\rho}$ values are significantly shifted from zero for all residues. This seems to suggest that there is a slow motion component affecting all the residues, and the magnitude of the R_{ex} term seems to be almost similar at all ^{13}C sites since most of the points cluster at the same height above the zero line.

The presence of a R_{ex} term for all the residues complicates the determination of global motion parameters from $R_{1\rho}/R_1$ ratios. The presence of a R_{ex} term in the numerator increases the ratio thereby affecting the estimates of overall correlation time and the $D_\parallel/D_\perp$ ratio. A possible solution to the problem is to estimate R_{ex} independently either by employing experimental methods or by calculations with the available data. The $R_{1\rho}/R_1$ ratios may then be corrected for the exchange contribution. We employed two methods to determine R_{ex} from C1′ relaxation data measured at two field strengths. Only C1′ data were used since the CSA contribution to relaxation is very small in comparison to the dipolar interaction. In the first approach (method 1), we consider the dipolar interaction dominates the relaxation process and introduce the quadratic dependence of the R_{ex} term on the field strength, so that the R_{ex} values can be determined from the difference of $R_{1\rho}$ rates at the two fields,

$$R_{ex} = \frac{R_{1\rho}^{(600)} - R_{1\rho}^{(500)}}{(600/500)^2 - 1} \quad (12)$$

We also estimated R_{ex} based on a more detailed approach (method 2), suggested for application to relaxation data in proteins. Camerero et al. derived an expression for estimating R_{ex} values from relaxation data of ^{15}N, measured at two static field strengths.[40] Adapting the same method to ^{13}C gives the following expression for R_{ex}.

$$R_{ex} = \frac{\omega_{(500)}^2}{2(\omega_{(600)}^2 - \omega_{(500)}^2)}\{X_{(600)}[1 + (4c_{(500)}^2/9d^2)] - X_{(500)}[1 + (4c_{(600)}^2/9d^2)]\} \quad (13)$$

where

$$X_{(\upsilon)} = 2R_{1\rho}^{(\upsilon)} - R_1^{(\upsilon)}[1 + 2.932(\mathrm{NOE}^{(\upsilon)} - 1)(\gamma_C/\gamma_H)] \quad (14)$$

and d and $c_{(\upsilon)} = (\sigma_\parallel - \sigma_\perp)^2\omega_C^2$ are the dipolar and CSA interaction constants. Since the equation was originally derived

(40) Camarero, J. A.; Fushman, D.; Sato, S.; Giriat, I.; Cowburn, D.; Raleigh, D. P.; Muir, T. W. *J. Mol. Biol.* **2001**, *308*, 1045–1062.

Table 2. Internal Motion Parameters for VTS1p−SRE-RNA[a]

	C2/C5/C8			C1′		
	S^2	τ_i (ps)	R_{ex} (s^{-1})	S^2	τ_i (ps)	R_{ex} (s^{-1})
G2	1.0 ± 0.14		44.4 ± 3.2	1.0 ± 0.014 (*1.0 ± 0.012*)		14.5 ± 0.76 (*14.2 ± 0.49*)
A3	0.908 ± 0.012		18.0 ± 0.14	1.0 ± 0.018 (*1.0 ± 0.017*)		15.1 ± 0.42 (*14.2 ± 0.31*)
G4	1.0 ± 0.013		19.8 ± 0.24	1.0 ± 0.016 (*1.0 ± 0.016*)		15.8 ± 0.33 (*14.7 ± 0.25*)
A5	0.878 ± 0.015		23.1 ± 0.27	1.0 ± 0.011 (*1.0 ± 0.012*)		15.2 ± 0.21 (*13.9 ± 0.17*)
G6	0.978 ± 0.016		17.0 ± 0.31	0.927 ± 0.011 (*0.968 ± 0.013*)	17.7 ± 1.8 (*17.3 ± 1.8*)	24.5 ± 0.19 (*20.6 ± 0.21*)
G7	0.861 ± 0.013		23.3 ± 0.14	1.0 ± 0.013 (*1.0 ± 0.012*)		16.1 ± 0.80 (*14.8 ± 0.68*)
C8	1.0 ± 0.019		13.2 ± 1.0	1.0 ± 0.016 (*1.0 ± 0.014*)		9.0 ± 1.00 (*8.3 ± 0.70*)
U9	0.797 ± 0.017		40.6 ± 0.13	0.880 ± 0.014 (*1.0 ± 0.015*)	35.1 ± 1.3	34.7 ± 0.17 (*27.1 ± 0.16*)
C10	0.896 ± 0.014	32.9 ± 1.7	15.0 ± 0.18	1.0 ± 0.016 (*1.0 ± 0.015*)		12.4 ± 0.22 (*12.0 ± 0.30*)
U11	0.804 ± 0.014	7.5 ± 1.5	21.2 ± 0.23	1.0 ± 0.011 (*1.0 ± 0.012*)		14.3 ± 0.12 (*12.9 ± 0.19*)
G12	0.887 ± 0.019		23.7 ± 0.18	0.849 ± 0.012 (*0.880 ± 0.012*)		16.9 ± 0.12 (*15.2 ± 0.11*)
G13	0.885 ± 0.013		23.8 ± 0.15	0.969 ± 0.013 (*1.0 ± 0.012*)	17.9 ± 2.0	14.2 ± 0.14 (*10.9 ± 0.19*)
C14						
A15	0.833 ± 0.018		25.6 ± 0.14	1.0 ± 0.012 (*1.0 ± 0.014*)		12.8 ± 0.11 (*11.8 ± 0.32*)
G16	0.944 ± 0.019		16.6 ± 0.17	0.926 ± 0.012 (*1.0 ± 0.004*)	39.8 ± 1.6	12.3 ± 0.13 (*9.8 ± 0.14*)
C17	0.787 ± 0.014	21.4 ± 1.4	29.6 ± 0.16	1.0 ± 0.017 (*1.0 ± 0.013*)		12.2 ± 0.32 (*12.1 ± 0.17*)
U18	1.0 ± 0.012		19.7 ± 0.19	0.882 ± 0.017 (*1.0 ± 0.016*)	43.8 ± 2.6	20.4 ± 0.39 (*12.9 ± 0.19*)
U19	0.832 ± 0.017	7.8 ± 1.4	27.8 ± 0.11	0.809 ± 0.013 (*0.925 ± 0.012*)	7.6 ± 0.8	24.5 ± 0.15 (*16.1 ± 0.15*)
U20				1.0 ± 0.018 (*1.0 ± 0.019*)		20.5 ± 0.13 (*21.5 ± 0.12*)
U21	0.851 ± 0.019		29.7 ± 0.15	0.941 ± 0.017 (*1.0 ± 0.012*)	35.5 ± 1.3	17.0 ± 0.15 (*12.8 ± 0.13*)
C22	0.858 ± 0.014	31.1 ± 1.3	23.4 ± 0.19	1.0 ± 0.012 (*1.0 ± 0.013*)		7.7 ± 0.32 (*8.7 ± 0.11*)
C23	0.847 ± 0.015		17.6 ± 0.18	1.0 ± 0.028 (*1.0 ± 0.037*)		8.2 ± 1.4 (*7.3 ± 1.6*)

[a] Values in parentheses are obtained by fitting relaxation data of C1′ at 500 and 600 MHz simultaneously.

in the context of ^{15}N spins in proteins for which CSA is assumed to be axially symmetric, we assumed a symmetric C1′ CSA tensor with ($\sigma_{||} - \sigma_{\perp}$) value of 40 ppm for the purpose of this calculation.[17] Since the method is applied only to C1′ carbons for which the contribution from CSA to relaxation is low, the assumption of axially symmetric CSA does not lead to large errors. Note that these approaches cannot be applied to aromatic carbons because of the large contribution from the asymmetric CSA to relaxation rates. The R_{ex} values determined by both these approaches is given in Table S2. The values obtained by both methods agree closely and implies that the simpler approach in method 1 for estimating R_{ex} is acceptable.

The R_{ex} values estimated using eq 12 were subtracted from the $R_{1\rho}$ values of the C1′ carbons to correct for the exchange contribution and utilized to obtain the $R_{1\rho}/R_1$ ratios for determining parameters for overall motion. As in the case of SRE-RNA, the ratios from the loop residues were excluded and the rotational diffusion parameters were determined from 16 exchange corrected $R_{1\rho}/R_1$ ratios from the 500 MHz data of C1′ carbons. The best fit to experimental ratios are obtained for ($\theta_{||}$, $\phi_{||}$) = (75°, 71°), overall rotational correlation time τ_c = 10.93 ns and a diffusion anisotropy of $D_{||}/D_{\perp}$ = 1.65 (Figure S4), which were used in subsequent calculations. These values compare favorably with the values obtained from *hydronmr*, ($\theta_{||}$, $\phi_{||}$) = (67°, 73°), τ_c = 10.12 ns and $D_{||}/D_{\perp}$ = 1.82.

The overall motion parameters were also determined by using $R_{1\rho}/R_1$ of aromatic and anomeric carbons at 500 MHz without applying any correction for exchange and excluding data from loop residues. This gives parameters ($\theta_{||}$, $\phi_{||}$) = (88°, 70°), τ_c = 12.69 ns and $D_{||}/D_{\perp}$ = 1.57. When overall motion parameters were set to these values, most residues still required a R_{ex} term for a good fit of the R_1, $R_{1\rho}$ and NOE data in the model-free analysis. Hence, a correction for exchange contribution seems to be necessary before determining the overall motion parameters. Since the large CSA makes it difficult to estimate R_{ex} contribution to relaxation of the aromatic carbons, we used only corrected C1′ data for determining parameters for rotational diffusion.

The parameters related to orientation and magnitude of the rotational diffusion tensor determined for SRE-RNA and VTS1p−SRE-RNA clearly reveals the change in hydrodynamics of the RNA when bound to the protein. This is also visible in comparing the pattern of relaxation rates across residues for the C1′ carbons (Figures 2 and 4), particularly R_1 rates which are not affected by exchange. The pattern of rates across residues reflect the distribution of C1′−H1′ bond orientations with respect to the molecular axis, with slight variations arising from differences in internal motion at individual anomeric sites. Similar trends are not obvious in aromatic carbon relaxation rates because the C−H bonds have only a narrow distribution about the perpendicular orientation. In addition the rates are also affected by the CSA orientation and magnitudes which differs for the different carbon types. The rotational diffusion parameters determined from experimental data are consistent with the values calculated using *hydronmr* based on the solution NMR structures of the free RNA and the RNA bound to the protein. In both cases the unique axis of the diffusion tensor is oriented lengthwise in the molecule.

Internal Motions. The global motion parameters determined from exchange corrected relaxation rate ratios of C1′ carbons were kept constant and internal motion parameters of the model-free formalism were determined from R_1, $R_{1\rho}$ and NOE data of each ^{13}C at 500 MHz. Relaxation data measured at 600 MHz did not have the benefit of a low temperature probe and the measurement errors in the rates were large for the aromatic carbons, especially for $R_{1\rho}$ due to fast relaxation. Hence 600 MHz data of aromatic carbons could not be used reliably in the analysis of internal motions. The internal motion parameters which give the best fit to the experimental data are given in Table 2. The relaxation rates calculated using these parameters are included in the Figure 4 along with the experimental points.

Internal motion parameters for C1′ carbons were also estimated by fitting simultaneously to R_1, $R_{1\rho}$ and NOE data at 500 and 600 MHz (Figure S5). These results are included in parentheses in Table 2. For most residues, parameters determined from relaxation data at single field or at two fields agree

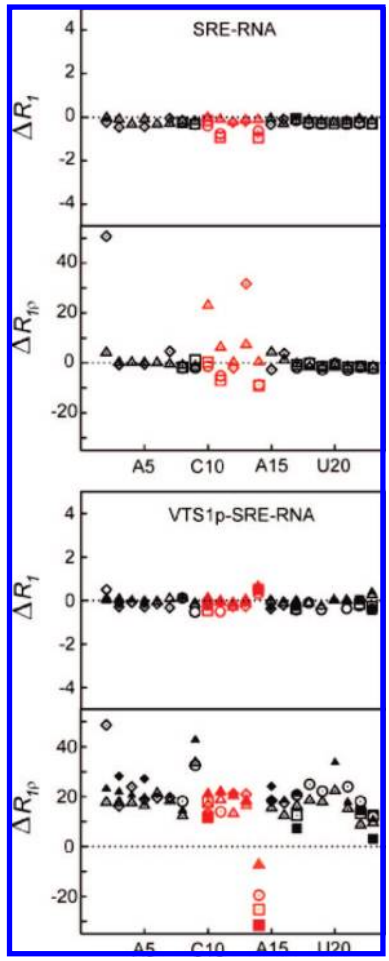

Figure 5. Comparison of the difference between experimental relaxation rates and rates calculated assuming axially symmetric rotational diffusion with no internal motions for SRE-RNA and VTS1p−SRE-RNA with open and full symbols referring to data at 500 and 600 MHz respectively. Symbols denoting different carbon types are indicated in Figure 1. Parameters corresponding to the rotational diffusion tensor were obtained from hydrodynamics calculations using *hydronmr* with the PDB structures of SRE-RNA and VTS1p−SRE-RNA.

well. Some residues show higher NOE values at 500 MHz but the NOE values measured at 600 MHz seem more uniform and for these residues some differences are observed in the internal motions parameters determined from data at a single or two static fields.

In VTS1p−SRE-RNA, in which the RNA is bound to the protein, the distinct difference between the nature of fast internal motions between the loop and stem region is no longer observed. Only relaxation data of fewer ^{13}C sites need to be fit to the more complex motional models 2 and 4, and the few sites which are fit by these models have a shorter correlation time for fast motions. In the stem region many of the ^{13}C sites in the nucleotide base, show a decrease in S^2 value compared to SRE-RNA whereas they increase for the anomeric carbons. The changes in amplitudes of fast motion occurring on binding are compared in Figure 6. The most interesting changes are observed in the loop and flanking residues. Both U9 and A15 residues which neighbors the loop show a considerable decrease in S^2 values on binding. A decrease in S^2 value is also observed for the anomeric carbon of U9. The increased mobility of the U9-A15 pair could be partly due to its proximity to the mobile residue C14. The relaxation data for the residue C14 could not be analyzed with models 1−4 and probably requires a more complex motional model. When examining the structure of the RNA bound to the protein, the C14 residue seems to have an orientation which allows considerable freedom of motion as observed in SRE-RNA. It is also interesting to note that electron density corresponding to the C14 nucleotide could not be observed in the crystal structure, indicating a disordered site.[7] Similar observation has been reported for residues C24 and U25 in the binding region of HIV-1 TAR RNA.[18] These residues show very different relaxation rates compared to the others, similar to what we observe for C14 and the S^2 values are found to decrease considerably in the ligand bound state. The residue G13 also shows a slight decrease in S^2 in the nucleotide base and both G13 and C10 show an increase in S^2 at the anomeric site. The residue which is the most significant in the recognition process, G12, shows a slight increase in S^2 for the base and a decrease in S^2 at the C1′ site. The S^2 value increases in U11 at both the aromatic and anomeric carbons, the former being considerable. The decreased mobility of U11 is expected because it has interactions with the protein in the bound form of the RNA.

The overall effect on binding seems to be that the amplitudes of fast motion increases in the nucleotide bases and decreases at the anomeric sites. Increased flexibility of base-pair steps involving a series of interdependent movements upon protein binding have been discussed in the context of DNA where it is expected to affect the entropy of complex formation.[41] It is possible that for the RNA in the bound form, the amplitudes of fast motion for the sugar moieties of the backbone are reduced due to the interactions between the phosphate oxygens and the protein residues in the binding site. The increased fluctuations of the base planes on the other hand would add to the entropy of the complex thereby influencing the free energy change of the protein−RNA interaction favorably. There is increasing evidence from dynamics studies of protein−ligand and protein−protein interactions that binding does not always lead to motional restriction.[42−44] An increase in the amplitude of fast motions throughout a protein has been observed on binding to a pheromone suggesting that increases in motion can dominate the free energy of association in certain cases.[45]

Slow Conformational Fluctuations. The dependence of $R_{1\rho}$ rates on the spin-lock field strength was examined for ^{13}C spins in VTS1p−SRE-RNA at 500 MHz. Spin-lock field dependence of rates is observed for ^{13}C sites of many more residues in VTS1p−SRE-RNA when compared to SRE-RNA. The data from residues for which fairly good fits are obtained using the fast exchange model in eq 11 are shown in Figure 7, and the fit parameters are listed in Table S3. In some cases, data could not be analyzed reliably due to scatter of points. Also, data for some of the ^{13}C sites do not give fits with reasonable parameters for the two site fast exchange model. It is however possible that a more complex model covering slow and intermediate exchange might be required for some residues, for example C10 and G13 which have comparatively flat profiles and exchange time scales of hundred μs or more whereas other sites have exchange times of tens of μs. The experiments which examine the changes in $R_{1\rho}$ rates with spin-lock field strength access the

(41) Olson, W. K.; Gorin, A. A.; Lu, X.- J.; Hock, L. M.; Zhurkin, V. B. *Proc. Natl. Acad. Sci. U.S.A.* **1998**, *95*, 11163–11168.
(42) Forman-Kay, J. D. *Nat. Struct. Biol.* **1999**, *6*, 1086–1087.
(43) Bouguet-Bonnet, S.; Buck, M. *J. Mol. Biol.* **2008**, *377*, 1474–1487.
(44) Arumugam, S.; Gao, G.; Patton, B. L.; Semenchenko, V.; Brew, K.; van Doren, S. R. *J. Mol. Biol.* **2003**, *327*, 719–734.
(45) Zidek, L.; Novotny, M. V.; Stone, M. J. *Nat. Struct. Biol.* **1999**, *6*, 1118–1121.

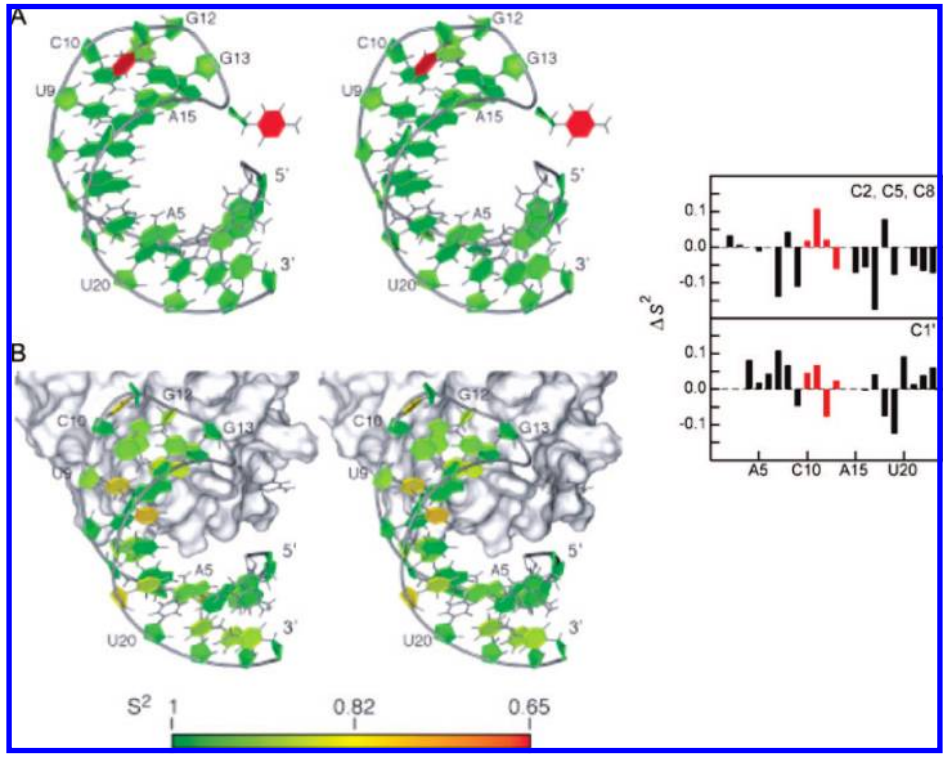

Figure 6. Stereo representation of SRE-RNA (A) and VTS1p−SRE-RNA (B) with base and sugar moieties color coded according to S^2 values of C2, C5, C8 and C1′ carbons. Green codes for less mobility and red codes for increased mobility as indicated by the scale below the figure. The graph shows the change in S^2 values at each carbon site of SRE-RNA on binding to the VTS1p-SAM domain.

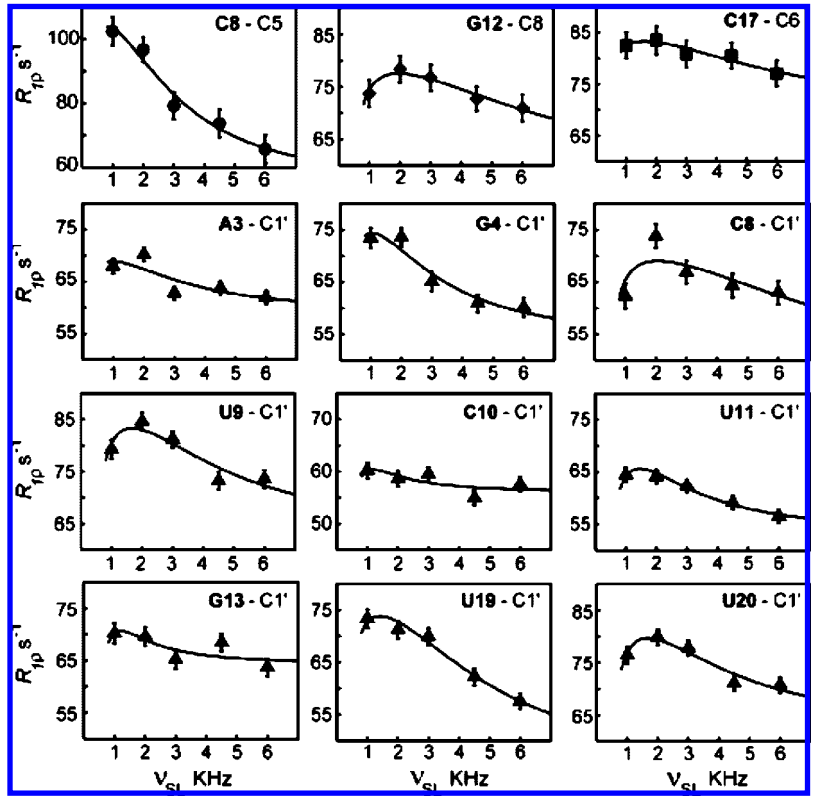

Figure 7. Fits of the two-site exchange model to the spin-lock field strength dependence of $R_{1\rho}$ rates for the aromatic and anomeric carbons of VTS1p−SRE-RNA.

exchange processes in the range of μs. A more detailed study of the exchange would require complementary experiments examining transverse relaxation rate dependence on the CPMG frequency which can access slow motions in the ms time scale[12,46,47] and spin-lock experiments employing weak radio frequency fields, which explores the exchange time scale

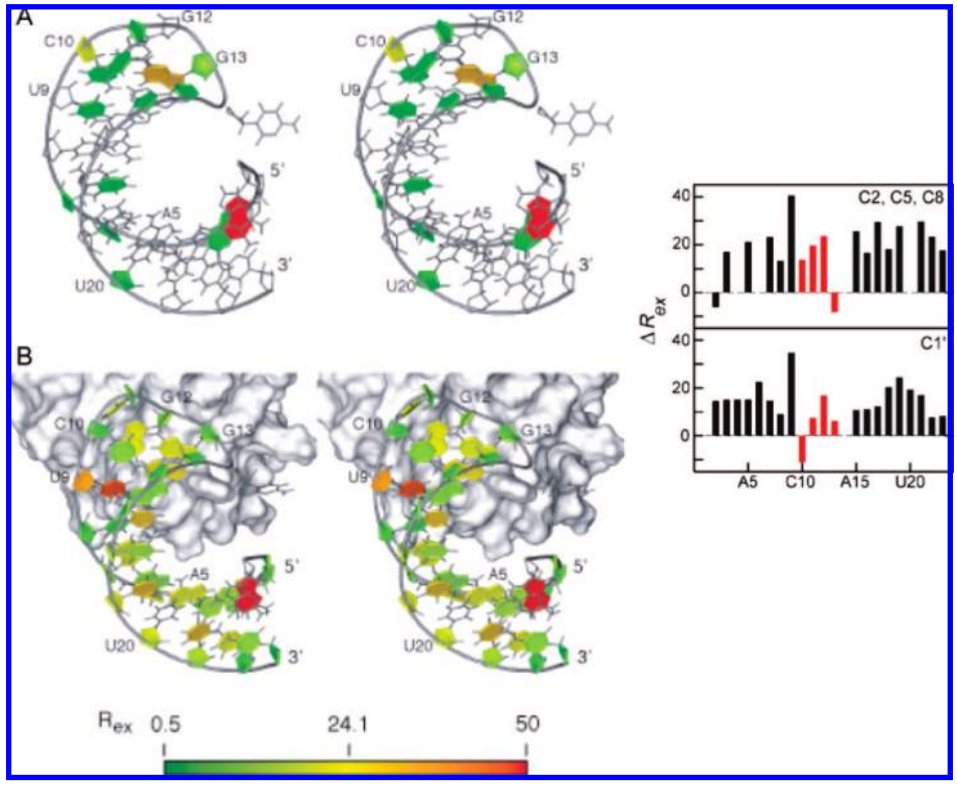

Figure 8. Stereo representation of SRE-RNA (A) and VTS1p−SRE-RNA (B) with base and sugar moieties color coded according to R_{ex} values of C2, C5, C8 and C1′ carbons, using a representation scheme similar to that of Figure 6. The graph shows the change in R_{ex} values at each carbon site of SRE-RNA on binding to the VTS1p-SAM domain.

window between the ones accessed by spin-lock field strength and CPMG frequency experiments.[48]

In contrast to SRE-RNA, a R_{ex} term is required to interpret the experimental data for all residues in the protein-bound RNA as seen from Figure 8. Many more sites in VTS1p−SRE-RNA show spin-lock dependence of the $R_{1\rho}$ rates and these are not necessarily confined to the loop and flanking residues. Except for the residues G2 and U9, all other ^{13}C sites show R_{ex} values in the range 10−30 s^{-1}. The average value observed for the aromatic sites is 21.6 ± 8 s^{-1} and for the anomeric sites 15.2 ± 8 s^{-1}. The observed values at individual sites could be partly a contribution from a net motion which affects the entire RNA with additional variations due to the differences in the nature of slow motions locally. One possibility for the exchange effect is that the RNA could be in exchange between the protein-bound and free forms in solution. However the observed R_1 rates are typical of a slowly tumbling macromolecular complex. Also, all spectra show only one set of peaks corresponding to the bound RNA. Hence, if there is an exchange between free and bound forms in solution, the fraction of RNA in the free form must be much less than that in the bound form.

Another possibility is that the RNA could be undergoing an overall collective slow motion within the binding cavity of the protein. A net collective motion in the ns time scale for one of the helical domains of an RNA bound to the U1A protein has been reported recently, in which the most crucial residue (A39) for protein recognition acts like a hinge point between parts of RNA that is bound to the protein and the domain that undergoes collective motion.[20] We observe similarities to those reported for A39 in the nature of binding induced dynamics changes at residue G12 which is crucial for recognition by the VTS1p-SAM domain. An unexpectedly high increase in $R_{1\rho}$ rates has also been observed across most of the residues in the case of HIV-2 TAR RNA on binding to a ligand.[19] It is possible that the increased slow time scale motions observed throughout the SRE-RNA on binding, is correlated to the corresponding increase in amplitudes of fast motion. The largest R_{ex} contributions are also observed for those sites at which the S^2 values are lower, for example in the U9-A15 base pair. A link between ps-ns backbone fluctuations and slower motions associated with catalytic activity has been demonstrated in proteins.[49] Increased mobility in both fast and slow time scales have been reported for a large number of residues in one of the partners involved in the binding of two well structured proteins, where the entropy increase dominates the unfavorable enthalpy of binding.[44] More recently, increased R_{ex} contribution has been observed for a large majority of residues in one of the partners following protein−protein binding with the values being uniform across residues in several regions.[43] It is possible that the fast and slow motions work together in the entropy contribution to the free energy of the protein−RNA interaction in the VTS1p−SRE-RNA system. Further experimental studies and computational modeling would be required to establish the coupling of fast and slow motional modes and its thermodynamics implications to the RNA−protein interaction process.

(46) Millet, O.; Loria, J. P.; Kroenke, C. D.; Pons, M.; Palmer, A. G., III *J. Am. Chem. Soc.* **2000**, *122*, 2867–2877.
(47) Mulder, F. A. A.; Mittermaier, A.; Hon, B.; Dahlquist, F. W.; Kay, L. E. *Nat. Struct. Biol.* **2001**, *8*, 932–935.
(48) Massi, F.; Johnson, E.; Wang, C.; Rance, M.; Palmer, A. G., III *J. Am. Chem. Soc.* **2004**, *126*, 2247–2256.
(49) Henzler-Wildman, K. A.; Lei, M.; Thai, V.; Kerns, S. J.; Karplus, M.; Kern, D. *Nature* **2007**, *450*, 913–918.

Dynamics Changes in the SRE-RNA Pentaloop. The changes in dynamics at individual sites may be examined in the context of the relevance of the various residues in the loop region to the recognition process. The structural studies have shown that G12 of the loop is the most important residue in the recognition process. G12 occupies the binding cavity and is the residue which makes maximum number of contacts with the protein through hydrogen-bonded interactions involving the amino and imino protons of the base and the oxygen of the phosphate group. The order parameter of the nucleotide base carbon of G12 increases on protein binding indicating a decrease in amplitude of fast motion (ps) of the base moiety. The order parameter at the anomeric site on the other hand decreases. This supports the observation of hydrogen-bonded interactions involving the G12 base in the protein-bound RNA structure. No indications of μs−ms motions were observed for the G12 residue in the free RNA but in the bound form G12 is subject to slow motions. It is significant that in the free RNA unlike other loop residues, G12 which is specifically recognized by the VTS1p-SAM domain has no slow conformational fluctuations, and the fast motions are also more restricted compared to other nonbase-paired residues of the loop.

Comparison of order parameters indicate that the flexibility of the base of G13 increases slightly in the bound form. The anomeric site however becomes more rigid for both C10 and G13. Both C10 and G13 have contacts to the protein through phosphate oxygens. The spin-lock field profiles for $R_{1\rho}$ rates of the anomeric carbons are also very similar in C10 and G13, suggesting their local dynamics are very closely related. The two residues are linked across the loop by a hydrogen bond, and this could explain the similarity of the local motions involving these residues. The C10-G13 base pairing is an essential feature which stabilizes the RNA fold. The residues C10, G12 and G13 are the most important for recognition by the VTS1p-SAM domain, and a mutation of any one of these residues drastically reduces the binding affinity.[50] These three residues form an arrangement very similar to those observed for nucleotides G25, C38 and A39 in the U1A protein−RNA complex.[20] The residue A39 which has stacking interactions with the G25-C38 base pair is the most significant residue in the recognition process. As observed in the case of G12 in VTS1p−SRE-RNA, A39 is comparatively rigid in the free RNA and on binding to U1A protein, the base becomes more rigid, whereas the anomeric site becomes more flexible.

The dynamics of residue U11 becomes considerably restricted in the protein-bound form when compared to the large amplitude motions of this residue in the free RNA. This residue also forms contacts with the protein through the phosphate group and is flanked by other residues which have significant contacts with the protein. Residue C14 on the other hand, has R_1 and NOE values in the bound form which are much higher than that observed for other residues while the $R_{1\rho}$ rates are lower, indicating that the carbon sites on C14 could be associated with considerably lower S^2 values. It is possible that the high freedom of motion of this residue in the free state is also retained to some extent in the bound form since it is looped out in the structure. The dynamics at this site probably needs to be analyzed in terms of a more complex model, for example the extension of the model-free approach which considers fast internal motions in two time scales, 10−200 ps and over 1000 ps.[51] Even though C14 has contact to the protein through the phosphate group, it is not essential in protein binding. Mutation or deletion of this residue does not have a strong effect on the binding.[50]The residue U9 which flanks the loop shows considerably increased mobility on protein binding. It is interesting that even though U9 is flanked by residues which have contacts to the protein, U9 itself does not make any specific contact with the protein. In general all residues which make contacts with the protein through the sugar−phosphate backbone show more restricted mobility at the anomeric site with the exception of G12.

Protein binding also results in significant contributions to the $R_{1\rho}$ relaxation rate from an exchange term. It is interesting to consider examples of other biomolecules in which a large number of residues show evidence of motions in the μs−ms time scale.[43,52] A striking example is that of RNase A in which almost one-third of the backbone residues show significant slow motions, many of them being located in the active site and substrate binding sites.[52] The exchange time scales were observed to be identical for all the residues within experimental error, suggesting a collective motion involving these sites. The presence of a collective slow motion in the μs−ms time scale in an RNA binding protein is interesting in the context of our observations for the protein-bound RNA. It is possible that the interface at which protein−RNA interactions occur is dynamic, with concerted slow motions over a continuously maintained and tightly packed interface. Interface dynamics have also been shown to be important in protein−DNA interactions.[53] As part of this project we are also carrying out studies of dynamics changes in the VTS1p-SAM domain on SRE-RNA binding which should throw more light on the nature of the binding interface dynamics. The dynamics of the VTS1p-SAM domain in the free form resembles that reported for RNase-A with restricted flexibility on the fast time scale (ps−ns) and mobility on the slower time scale at various regions some being located close to the binding region. Further work examining changes in the dynamics on RNA binding is in progress.

Conclusions

Relaxation rates for C2, C5, C6 and C8 nuclei of the nucleotide bases and the C1′ carbons of SRE-RNA in the free and protein-bound states have been analyzed assuming axially symmetric rotational diffusion for the overall motion and a model-free description of the internal motion, by including all relevant spin interactions. Quantitative analysis of the dynamics of the SRE-RNA in its free form and in the protein-bound state indicates that molecular motions play an important role in its recognition by the VTS1p-SAM domain. One of the important observations is that in the free RNA the nucleotide which is specifically recognized by the protein is fairly rigid in a loop, whereas other non-hydrogen-bonded residues are highly flexible. This has also been noted for nucleotides specifically recognized by proteins in few of the other dynamics studies of RNA−protein/ligand complexes and could be a significant feature in RNA−protein recognition. In most residues, flexibility seems to increase at the aromatic carbon sites while it decreases at the anomeric sites.

(50) Aviv, T.; Lin, Z.; Lau, S.; Rendl, L. M.; Sicheri, F.; Smibert, C. A. *Nat. Struct. Biol.* **2003**, *10*, 614–621.
(51) Clore, G. M.; Szabo, A.; Bax, A.; Kay, L. E.; Driscoll, P. C.; Gronenborn, A. *J. Am. Chem. Soc.* **1990**, *112*, 4989–4991.
(52) Cole, R.; Loria, J. P. *Biochemistry* **2002**, *41*, 6072–6081.

Much of the dynamics changes noted for the nucleotides of the pentaloop which forms the binding interface with the protein are consistent with the establishment of direct contacts with the protein sidechains. The surprising observation is the presence of significant slow motions in the RNA in its protein-bound form. The role of slow motions have not been analyzed quantitatively in the other reported dynamics studies of RNA−protein/ligand complexes. However, such enhanced slow motions of entire domains on binding have been observed in protein−protein interactions and has been suggested from detailed analysis of several DNA−protein structures. Since SRE-RNA binding to VTS1p-SAM domain does not involve significant structural changes in either partner, it is possible that enhanced flexibility in the bound state contributes toward making the association an entropy-driven process.

Acknowledgment. This work was supported by the Indo-Swiss Bilateral Research Initiative (ISBRI) program, a research grant to S.R. from the Department of Science and Technology, India, and grants from the Swiss National Science Foundation (Nr: 3100A0-118118) and from the Structural Biology National Center of Competence in Research (SNF-NCCR) to FHTA.

Supporting Information Available: Figures showing experimental and calculated relaxation data for C6 carbons, fits to anisotropic rotational diffusion model, multiple field experimental and calculated relaxation data for C1′ carbons and tables of calculated exchange rates and fit parameters for spin-lock field dependence of transverse relaxation rates.This material is available free of charge via the Internet at http://pubs.acs.org.

JA8023115

(53) Kalodimos, C. G.; Boelens, R.; Kaptein, R. *Chem. Rev.* **2004**, *104*, 3567–3586.